Analysis of an Electric Vehicle Charging System along a Highway*

Davide Cerotti[1], Simona Mancini[1], Marco Gribaudo[2], and Andrea Bobbio[1]

[1] Università del Piemonte Orientale, Alessandria, Italy
davide.cerotti,simona.mancini,andrea.bobbio@uniupo.it
[2] Politecnico di Milano, Milano, Italy
marco.gribaudo@polimi.it

Abstract. To reduce carbon emission, the transportation sector evolves toward replacing internal combustion vehicles by electric vehicles (EV). However, the limited driving ranges of EVs, their long recharge duration and the need of appropriate charging infrastructures require smart strategies to optimize the charging stops during a long trip. These challenges have generated a new area of studies that were mainly directed to extend the classical Vehicle Routing Problem (VRP) to a fleet of commercial EVs. In this paper, we propose a different point of view, by considering the interaction of private EVs with the related infrastructure, focusing on a highway trip. We consider a highway where charging stations are scattered along the road, and are equipped with multiple chargers. Using Fluid Stochastic Petri Nets (FSPN), the paper compares different decision policies when to stop and recharge the battery to maximize the probability of a car to reach its destination and minimize the trip completion time.

Keywords: Electric Vehicle, Charging infrastructure, Battery charge decision policy, Fluid Stochastic Petri Nets

1 Introduction

According to the Fuel Report 2021 of the International Energy Agency [1] the transport sector is responsible for around 60% of total oil demand. Inside the transport sector, oil was the predominant energy source, providing 92% of final energy over the past decade [2]. A major way to limit carbon emission in the transport sector is to replace internal combustion engine vehicles (ICEV) by electric vehicle (EV), and many countries are introducing new regulations and incentives to push the market toward this goal.

Between the two EV technological alternatives: hybrid electric vehicle (HEV) and battery electric vehicle (BEV), we consider, in the present paper, only BEV which are exclusively powered from rechargeable batteries mounted inside the vehicle. From the carbon emission point of view, BEVs have the following benefits as compared to ICEVs [3].

* Research partially supported by CNIT (Consorzio Nazionale Interuniversitario per le Telecomunicazioni).

- They reduce oil consumption, and greenhouse gas emissions, improving air quality.
- They operate with minimal noise.
- Can be charged from a wide range of different primary (renewable) energy sources, reducing kilometric cost.

On the other hand, their high cost of acquisition, limited driving ranges, the need for specific charging infrastructure, and long recharge duration limit the penetration of EV in the market.

The appearance of BEVs in the private as well in the commercial sector poses new challenges for their use and for the new infrastructures they need. These challenges have generated a new area of studies denoted as green logistic [4]. The major effort in this direction was to extend the classical Vehicle Routing Problem (VRP) to a fleet of commercial EVs and is referred to as Electric Vehicle Routing Problem (EVRP) [5]. The present paper, however, assumes a different point of view, considering a flow of private vehicles traveling along a highway and we study the performability of the system formed by the BEVs and the related infrastructure.

More specifically, we consider a long stretch of a highway with a flow of cars, both BEVs and non-BEVs, driving on it. A number of charging stations is scattered along the road and each charging station has one or more chargers. The problem of optimizing the siting and sizing of the charging infrastructure has been the object of recent research [6,7], but we assume here that the stations are already located and their positions are parameters to feed the model. We tag and follow a particular BEV that enters the highway at the beginning of the stretch and drives up to the end. We study the probability that the tagged car arrives at the end of its itinerary and the distribution of the time to complete the itinerary. The battery of the BEVs discharges as a function of the time, the speed of the car and the driven kilometers, while for the charging we adopt the non-linear function discussed in [8].

We model the system by means of a Fluid Stochastic Petri Net (FSPN) [9], in which the battery is represented by a fluid place with one input and one output fluid transition representing the charging and the discharging process, respectively.

The time that the tagged car takes to drive the segment between two successive service stations is a generally distributed random variable with a know mean (determined by the average speed of the car). The BEVs arriving at a charging station queue up for charge, and we assume, in the present formulation, that their arrival and service times are exponentially distributed. When the tagged driver arrives at a charging station she must decide whether to stop and recharge or go on. This decision depends on the level of the battery, the presence and the length of a queue at the station and the distance to the next station or to the destination. Different decision policies are considered and analyzed, also in view of a possible experimentation on autonomous EVs. The FSPN is solved analytically using Matlab, and a number of numerical experiments are presented to compare different decision policies.

The paper is organized as follows. In Section 2 we summarize the state of the art, in Section 3 the characteristics of the charging infrastructure and of the flow of cars are described. Section 4 illustrates the FSPN model, with the charging decision policies. The subsequent Section 5 sketches the numerical solution through a semi-discretization approach. Section 6 reports the numerical results and in Section 7 a discussion on the model and hints for future work close the paper.

2 State of the art

The diffusion of EVs is limited, especially in Italy with respect to other countries (Germany, France), also as a consequence of the scarcity of charging stations along the road network, and to their uneven distribution in the national territory. Although the technological innovation continuously increases the driving range of EVs, planning the charging stops is still a critical issue due to the long charging times. The seminal paper of Erdogan & Miller-Hooks [5] has first introduced the EVRP, considering different alternative-fuel vehicles (not only powered by electricity but also by GPL, hydrogen, natural gas etc.) for which the charging stations are not widespread on the territory. The paper generated a huge interest in the scientific community, and many extensions have been proposed and studied in the following years, as documented in two recent survey papers [10, 11].

Hybrid vehicles, which can switch from the electric propulsion to a traditional fuel have been addressed in [12]. Schneider et al., [13] introduced the EVRP with Time Windows (EVRPTW) in which customers must be visited within a prefixed time-window. The concept of partial recharges to the EVRPTW was introduced in [14], while in [15] a non-linear charging function is considered. In [16], charging stations with limited capacity are addressed for the first time, and a maximum number of vehicles that can simultaneously access the station is strictly imposed. Instead, in [17], vehicles are allowed to access the station and queue up if all the charging slots are busy, so that service may start when the queue becomes empty. All the above mentioned papers deal with decision problems faced by the usage of commercial EVs in freight distribution. In the present paper, we look at the problem under a different perspective considering a private BEV driver, immersed into a flow of private vehicles, who has to cover a given trip and must decide where and when to stop to recharge her vehicle to maximize the probability of completing the trip minimizing the total trip time. We introduce, in this paper, a performability view on the interaction between the EVs and the charging infrastructure [18], since we combine the evaluation of the driver trip time with the evaluation of the probability that the trip fails and the car does not complete its itinerary. The key element in the interaction between EVs and the infrastructure is the discharging and charging process of the battery. The flow intensity of the vehicles, the traffic conditions on the road and the queue length in front of a station are non-deterministic phenomena that can be represented by a stochastic model. To combine in a single framework the continuous variation of the charging level of the battery in time and the

randomness in the traffic condition, we model the system by means of a Fluid Stochastic Petri Net (FSPN) [9,19,20] where the battery is represented by a fluid place whose fluid level is the charge, the time to travel the highway between two successive service stations is a random variable with general distribution and the queue at a station is a M/M/γ if the station has γ parallel chargers.

FSPNs were introduced in [19] and further extended in [20]. FSPNs evolve the stochastic Petri nets framework [21] by introducing as new primitives the continuous places, which contain a fluid quantity, and the fluid arcs, which connect timed transitions to fluid places and determine the flow in and out to the fluid places. The basic FSPN formalism was enriched in [9] by introducing fluid impulses that increment the fluid level by a discrete quantity whose intensity depends both on the fluid levels and on the discrete marking of the net. FSPNs have a graphical representation that helps building the model, and then from the graphical representation we can derive the fluid stochastic equations that describe the underlying stochastic marking process. In general, the solution of these equations is a challenging task. Steady-state solution of FSPN models, with dependency on discrete places only, has been proposed in [20] using *spectral decomposition*. In the same paper, transient analysis has also been described using *upwind semidiscretization*. FSPNs have been successfully used in the literature to study systems in several technological areas, but we are not aware of applications in the field of EV routing.

3 The infrastructure and the EV

To be concrete, we consider, the Italian motorway A14 from Bologna to Taranto (743 km), which we display in Figure 1 with the real allocation of the service stations. The portion of highway between two charging stations is called segment. Table 2 in Appendix shown the location of the service stations along A14 Bologna to Taranto. We assume that each service station is equipped (or will be equipped in the near future) with a charging point with a number γ of parallel chargers and that all the chargers provide the same power, so that the charging profile is the same for all the EVs in all chargers.

Along the highway runs a flow of cars, composed by BEVs and non-BEVs and by the tagged BEV that we follow from the beginning of the trip up to the end. The other BEVs in the flow may compete for the charging points, generating possible queues at the stations when the tagged car arrives for charge. The non-BEV cars are not explicitly modeled, but their presence is reflected on the average speed of the car flow including the tagged BEV. The time that the tagged BEV takes to complete one segment is a random variable whose distribution may change in each road segment. The distribution of the driving time to complete a segment is modeled by a shifted Erlang distribution whose parameters (shift, expected value and number of stages) are input data (see Section 4) that may depend on the traffic conditions in the segment. In this way, we allow to model fluctuations or congestion in the traffic flow in specific segments of the highway. Each station is provided with γ parallel chargers and we assume that the BEVs

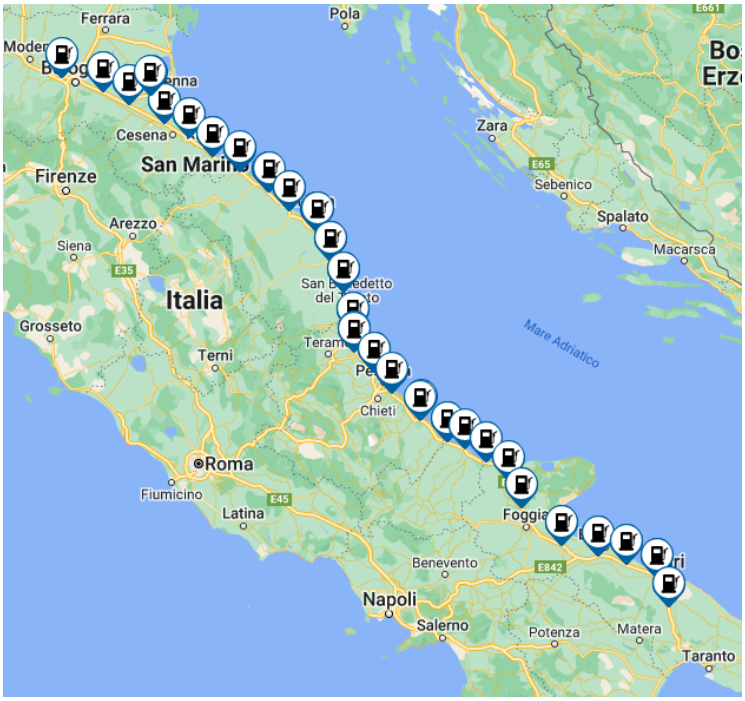

Fig. 1: The A14 from Bologna to Taranto with the actual position of the service stations. We assume that in each service station there is an EV charging point

arrive at the station according to a Poisson process of known parameter. In the present study, we assume also that all the BEVs and all the chargers have the same characteristics; furthermore we do not model the level of the residual charge of the vehicles joining the queue, hence, even if the charging profile has a nonlinear behavior (see Section 4.1), we approximate the charging time of the non-tagged BEVs at a station with an exponential distribution of known parameter, so that the queue in front of the station becomes a M/M/γ.

4 Fluid Stochastic Petri Net: The Scenario

Figure 2 shows the FSPN of the considered scenario. Following the customary notation for FSPNs [9, 20], the set of places $\mathcal{P}$ is partitioned in a set of discrete places $\mathcal{P}_d$ and a set of continuous places $\mathcal{P}_c$. Discrete places are drawn as single circles and may contain a discrete number of tokens, while continuous places are depicted by two concentric circles and contain a continuous quantity called fluid. The model of Figure 2 contains a single fluid place β representing the battery whose fluid level, ranging in the interval $0 \leq \beta \leq B$, is the charge measured in km.

The set of transition $\mathcal{T}$ is partitioned into a set of timed transitions $\mathcal{T}_E$, a set of immediate transitions $\mathcal{T}_I$ and a set of fluid transitions $\mathcal{T}_F$. Timed transitions are drawn as a rectangle and are assigned a random firing time with known distribution, immediate transitions are represented by a thin bar and fire in zero time, while fluid transitions are represented by double rectangles and connect the fluid places. In Figure 2, the timed transition *SEGMENT*(ϕ) (in gray) is assigned a general distribution, while transitions *EMP_Q* and *FREE*, representing the queue of BEVs at a station, have an exponentially distributed firing time. *B_UP* and *B_DOWN* are the fluid transitions modeling the charge and discharge of the battery, respectively,

The set of arcs $\mathcal{A}$ is partitioned into two subsets $\mathcal{A}_d$ and $\mathcal{A}_c$: the former is a subset of $(\mathcal{P}_d \times \mathcal{T}) \cup (\mathcal{T} \times \mathcal{P}_d)$ representing the discrete arcs and are drawn as single arrows, the latter is a subset of $(\mathcal{P}_c \times \mathcal{T}_F) \cup (\mathcal{T}_F \times \mathcal{P}_c)$ representing the fluid arcs and are drawn as double arrows. In Figure 2, the fluid arc from *B_UP* to β continuously adds fluid (charge) when enabled, while the fluid arc from β to *B_DOWN* continuously removes fluid when enabled. Inhibitor arcs, represented with dashed lines ending by a small circle, have the usual meaning of preventing a transition to fire when the input place contains a number of tokens (or a fluid level) greater or equal to the weight. In Figure 2, there are two inhibitor arcs: from place ϕ to transition *AVAIL_SLOT* which may fire only when place ϕ contains less than K tokens and from fluid place β to transition *FAIL* which may fire when the fluid level is less than the weight $l(\phi)$. Finally, impulse arcs, which connect fluid places to discrete transitions, add or remove a finite amount of fluid during the firing event. In Figure 2, the only impulse arc is from place β to transition *SEGMENT*(ϕ), and removes a fluid quantity $l(\phi)$ when the transition fires.

Let $\mathbf{m}_i = [\#p_i, i \in \mathcal{P}_d]$ be the discrete marking of the FSPN and let $\mathbf{x}$ be the vector of the fluid levels in the continuous places. The complete state of the fluid Petri net is given by the pair $M = (\mathbf{m}_i, \mathbf{x})$ which evolves in time, generating the stochastic marking process $\mathcal{M}(\tau) = \{(\mathbf{m}_i, \mathbf{x}), \tau \geq 0\}$. The evolution of each fluid level x depends both on a continuous component determined by the instantaneous flow rates assigned to fluid arcs and a discrete component determined by fluid impulses transferred to (or removed from) the fluid place when the impulse transition fires [9].

Place N represents the tagged car initiating segment ϕ, with $\phi = 1, ..., \boldsymbol{K}$, counted in place ϕ. The total number of segments to be traveled is hence denoted by $\boldsymbol{K}$. Transition *SEGMENT*(ϕ) represents the completion of segment ϕ and the arrival at the charging station at the end of the segment. Such transition is characterized by a state-dependent shifted-Erlang firing time, expressed by Equation (1), where s is the number of exponential stages, t_0 the shift and ψ the rate parameter.

$$f(t) = \begin{cases} \dfrac{\psi^s (t - t_0)^{s-1} e^{-\psi(t-t_0)}}{(s-1)!} & t \geq t_0 \\ 0 & t < t_0 \end{cases} \tag{1}$$

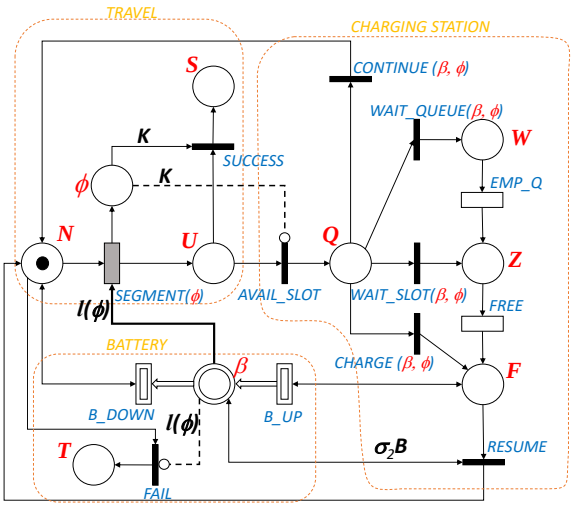

Fig. 2: Fluid Stochastic Petri Net model of the considered scenario.

Let l_ϕ be the length of segment ϕ, $v_{\max}$ the maximum speed allowed for the car, and v_{ave} the average speed on the segment. t_0 and ψ are defined as follows:

$$t_0 = \frac{l_\phi}{v_{\max}} \quad ; \quad \psi = \frac{s}{l_\phi \left(\frac{1}{v_{\text{ave}}} - \frac{1}{v_{\max}} \right)} \tag{2}$$

The distribution (1) starts at t_0, which is the traveling time when the segment is driven at the maximum speed $v_{\max}$, and the expected value is $E[t] = \frac{l_\phi}{v_{\text{ave}}}$ as required by the definition of v_{ave}. From Equations (2), the parameters t_0 and ψ of the distribution (1) are derived assigning $v_{\max}$ and v_{ave}, while the number of stages s is assigned independently.

The coefficient of variation c_v is lower than the corresponding non-shifted Erlang with same order s:

$$c_v = \frac{1}{\sqrt{s}} \left(1 - \frac{v_{\text{ave}}}{v_{\max}} \right) \tag{3}$$

4.1 The Battery level

In the control screen of most EVs, the battery level is conventionally measured and displayed in kilometers. The battery is consumed during the firing time of transition *SEGMENT(ϕ)* (when a token is in place *N*) according to distribution in (1), and charges when a token is in place *F*. Battery charging and discharging are modeled by fluid transitions *B_UP* and *B_DOWN*, respectively. The discharge is a function of the length l_ϕ of segment ϕ, the average speed of the car

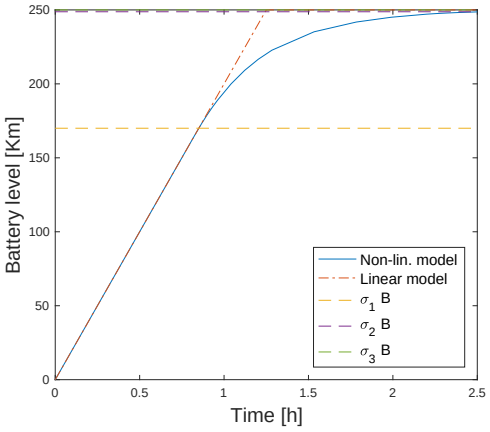

$$\frac{d\beta}{dt} = \begin{cases} r_c & ; \quad \beta < \sigma_1 B \\ r_c \cdot \dfrac{\sigma_3 - \beta/B}{\sigma_3 - \sigma_1} & ; \sigma_1 B \leq \beta < \sigma_2 B \\ 0 & ; \quad \beta \geq \sigma_2 B \end{cases} \tag{4}$$

Fig. 3: The non linear charging profile

and of the power supplied to support services such as air conditioning and music playing (converted in equivalent km), which is a function of the time spent to drive segment ϕ. The rate of consumption of the battery increases almost linearly with the average speed [22] beyond a cruise speed of around 50 km/h.

For each segment we could assign a value for $v_{\max}$ and v_{ave} to define the distribution of the time to drive the segment. However, in the present paper we keep the same values of $v_{\max}$ and v_{ave} for all the segments, but we show how the model reacts modifying these values. The random time to drive a segment is given by t_0 (the time to drive the segment at the maximum speed), augmented by the deviation given by the Erlang component (the series of s exponential stages) (Equation 1). During this period, the battery level β reduces at a rate $r(t,i) = -r_b$ to account for the services. At the end of the last Erlang stage, transition *SEGMENT(ϕ)* fires and a fluid impulse l_ϕ, reduces the battery level to account for the completion of segment ϕ.

When a token is in place F, the battery charges according to a non-linear model inspired by the work in [8]. The recharge model is given by Equation (4), where r_c is the initial constant recharge rate and σ_i are the parameters needed to define the non-linear behavior. Figure 4 gives the corresponding non linear charging profile. As soon as the capacity $\sigma_2 B$ is reached, immediate transition *RESUME* fires, putting a token in place N to prepare for driving the next segment. Whenever the battery level β becomes zero or negative, due to the reduction at rate r_b or to the effect of the negative impulses, the immediate transition *FAIL* is triggered causing the mission to fail. This is modeled with the inhibitor arc of weight l_ϕ that connects β to FAIL.

When transition *SEGMENT*(ϕ) fires and $\phi = \boldsymbol{K}$ (last segment), transition *AVAIL_SLOT* is disabled, immediate transition *SUCCESS* fires and the tagged car successfully completes its itinerary. If $\phi < \boldsymbol{K}$ transition *AVAIL_SLOT* fires

and place Q becomes marked, the tagged BEV must take the decision whether to continue, or to stop and recharge. This decision is performed inside the element of the *CHARGING STATION* box of Figure 2, and depends on the current battery level β, on the position of the car ϕ, on the state of the queue and on the implemented stopping decision policy.

We have modeled the queue at the charging stations as a M/M/γ and we have computed its state probabilities. We define p(Wait) the probability that the chargers are busy and there is a queue in front, p(NoQueue) the probability that the chargers are busy, but there are no cars in the queue, and p(Free) the probability that there are empty slots. Such probabilities can be computed from the queue length distribution $\pi_{Q(n)}$ using the conventional formula [23]:

$$\rho = \frac{\lambda}{\gamma\mu}, \qquad \pi_{Q(n)} = \begin{cases} \frac{\pi_{Q(0)}}{n!} \cdot (\gamma\rho)^n & n < \gamma \\ \frac{\pi_{Q(0)}\gamma^\gamma\rho^n}{\gamma!} & n \geq \gamma \end{cases} \tag{5}$$

$$\pi_{Q(0)} = \left[\frac{(\gamma\rho)^\gamma}{\gamma!} \frac{1}{1-\rho} + \sum_{k=0}^{\gamma-1} \frac{(\gamma\rho)^k}{k!} \right]^{-1} \tag{6}$$

$$p(\text{Free}) = \sum_{n=0}^{\gamma-1} \pi_{Q(n)}, \qquad p(\text{NoQueue}) = \pi_{Q(\gamma)}, \qquad p(\text{Wait}) = 1 - \pi_F - \pi_Z \tag{7}$$

where λ is the arrival rate of BEVs at the station and $1/\mu$ is the average time to recharge. The resulting values, together with the chosen stopping decision policy, are then used to compute the firing probabilities of the four immediate transitions *CONTINUE*, *WAIT_QUEUE*, *WAIT_SLOT* and *CHARGE*, as detailed in Section 4.3.

4.2 Stopping Decision Policies

In the present paper, we take into account only the waiting and service times due to the queue and we neglect the overhead in exiting the highway, pulling up to a charger, plug in, and then reentering the highway. This overhead can be easily introduced in the FSPN of Figure 2 by adding an extra timed transition if the car decides to stop at a station.

We experiment different stopping decision policies where each policy j is characterized by three functions that return the probability of stopping depending on the current battery level β, and the distance of the next charging stations (derived from the segment ϕ): *i)* if there are free slots $u_f^{[j]}(\beta, \phi)$ (token in place *F*), *ii)* if the slots are busy, but there are no cars queuing, $u_z^{[j]}(\beta, \phi)$ (token in place *Z*) and *iii)* if there are already other cars queuing for a charging facility to become free $u_w^{[j]}(\beta, \phi)$ (token in place *W*).

We have tested five different stopping policies:

1. **Stop only when absolutely needed**: stop only if the remaining battery level is not enough to reach the next charging station. This policy is implemented with the following functions:

$$u_f^{[1]}(\beta,\phi) = \mathbf{1}(\beta < l_{\phi+1})$$
$$u_z^{[1]}(\beta,\phi) = \mathbf{1}(\beta < l_{\phi+1})$$
$$u_w^{[1]}(\beta,\phi) = \mathbf{1}(\beta < l_{\phi+1})$$

   where $\mathbf{1}(\bullet)$ is the indicator function that returns 1 if proposition $\bullet$ is true, 0 otherwise.
2. **Blind probabilistic stopping**: stop at any station, independently of the queue, with a given probability p:

$$u_f^{[2]}(\beta,\phi) = p$$
$$u_z^{[2]}(\beta,\phi) = p$$
$$u_w^{[2]}(\beta,\phi) = p$$

3. **Informed probabilistic stopping**: stop at any station, with a given high probability p_e if there is at least an empty slot, or with a lower probability p_w if there is to wait:

$$u_f^{[3]}(\beta,\phi) = p_e$$
$$u_z^{[3]}(\beta,\phi) = p_w$$
$$u_w^{[3]}(\beta,\phi) = p_w$$

4. **Avoid waiting**: We define a safety threshold of η km. Whenever the battery level β is such that $(\beta < \eta)$, stop if there is at least a free charger, otherwise retry at the next station. However, if the remaining battery level is less than the length of the next segment, stop anyway.

$$u_f^{[4]}(\beta,\phi) = \mathbf{1}(\beta < \eta)$$
$$u_z^{[4]}(\beta,\phi) = \mathbf{1}(\beta < l_{\phi+1})$$
$$u_w^{[4]}(\beta,\phi) = \mathbf{1}(\beta < l_{\phi+1})$$

5. **Skip long queues**: This policy relaxes the previous one, by allowing the car to stop with probability p, even if all chargers are busy, but there are no other cars in the queue.

$$u_f^{[5]}(\beta,\phi) = \mathbf{1}(\beta < \eta)$$
$$u_z^{[5]}(\beta,\phi) = p \cdot \mathbf{1}(\beta < \eta)$$
$$u_w^{[5]}(\beta,\phi) = \mathbf{1}(\beta < l_{\phi+1})$$

Of the proposed policies, the first three are just for comparison purpose, since they are not realistic; the ones on which this work really focuses are the last two.

4.3 Computing Decision Policy Probability

As transition *AVAIL_SLOT* fires depositing a token in place Q four immediate competing transitions are enabled determining the next move of the tagged car. The weights of the four immediate transitions are a function of the state of the queue and the stopping policy j and are computed as:

$$w_{CONTINUE} = \\ p(\text{Free})(1-u_f^{[j]}) + p(\text{NoQueue})(1-u_z^{[j]}) + p(\text{Wait})(1-u_w^{[j]}) \tag{8}$$

$$w_{WAIT\_QUEUE} = p(\text{Wait})u_w^{[j]} \tag{9}$$

$$w_{WAIT\_SLOT} = p(\text{NoQueue})u_z^{[j]} \tag{10}$$

$$w_{CHARGE} = p(\text{Free})u_f^{[j]} \tag{11}$$

In Equations (8) to (11) the dependencies on β and ϕ have been omitted to simplify the presentation. If there is a queue of cars already waiting to be served the waiting time is modelled by transition *EMP_Q(γ)*, which, according to queuing theory [24], is exponentially distributed with rate:

$$q_{\text{EMP\_Q}(\gamma)} = \gamma\mu - \lambda \tag{12}$$

If all slots are full, but there are no other cars in the queue, the waiting time represented by transition *FREE*(γ), is exponentially distributed with rate:

$$q_{\text{FREE}(\gamma)} = \gamma\mu \tag{13}$$

When a token arrives in place F, the charging of the battery begins. If, instead, the decision is to continue, the immediate transition *CONTINUE* fires, moving the tagged BEV to the next segment.

5 Solution Equation

Since there is only one fluid place with fluid level β, the stochastic marking process of the FSPN of Figure 2 can be written as (see Section 4) $\mathcal{M}(t) = \{(\mathbf{m}_i, \beta), t \geq 0\}$. The non exponential distribution of transition *SEGMENT(ϕ)* is modeled with a phase-type approach, and the discrete marking $\mathbf{m}_i$ includes both the s stages of the shifted Erlang distribution and the state of the queue.

Then, let us define $\pi_i(t, \beta)$ as the probability density of finding the system in state $\mathbf{m}_i$ with fluid level β at time t, q_{ij} as the transition rates from state $\mathbf{m}_i$ to state $\mathbf{m}_j$ and d_{ij} as the fluid impulse transferred to the fluid place at the transition firing from state $\mathbf{m}_i$ to state $\mathbf{m}_j$. In our case, q_{ij} corresponds either to the rates of the Erlang stages given in Equation (2), to the rates given in Equations (12) or (13), or to a Dirac's delta on the fluid component to represent the battery level dependent jumps caused by either end of charging or failure.

The fluid impulse terms are $d_{ij} = -l_\phi$ for the transitions at the end of the Erlang stages, and $d_{ij} = 0$ otherwise.

The transient behavior of the model illustrated in Section 4 follows the system of partial differential equations:

$$\frac{\partial \pi_i(t,\beta)}{\partial t} - \frac{\partial \left(r(t,i,\beta)\cdot \pi_i(t,\beta)\right)}{\partial \beta} = \sum_{\mathbf{m}_j \in \mathcal{M}_d, \mathbf{m}_j \neq \mathbf{m}_i} q_{ji}\pi_i(t,\beta + d_{ij}) \ , \quad \forall \mathbf{m}_i \in \mathcal{M}_d. \tag{14}$$

We apply a semi-discretization of (14) in the coordinate direction β using a first-order upwind method [20]. Since the fluid place of the battery is bounded at a maximum level B, its fluid level can be discretized at a finite number of equidistant points $\beta_i = i\Delta\beta$ with $0 \leq i \leq \lfloor \frac{B}{\Delta\beta} \rfloor$, where $\Delta\beta$ is the size of the discretization interval of the battery level.

From the semi-discretization we obtain the linear system of ordinary differential equations:

$$\frac{d\tilde{\boldsymbol{\pi}}(t)}{dt} = \tilde{\boldsymbol{\pi}}(t)(\tilde{\boldsymbol{Q}} + \tilde{\boldsymbol{W}}), \tag{15}$$

where $\tilde{\boldsymbol{\pi}}(t)$ is the vector of the probabilities that the system is in a discrete marking at different points of the discretized fluid range, $\tilde{\boldsymbol{Q}}$ is the state transition matrix representing the discrete part of the net and $\tilde{\boldsymbol{W}}$ is the discretization of the space derivative multiplied by the flow rates; more details can be found in [20].

Such equations can be integrated and solved by any standard method. In particular, we resorted to the `ode23()` function of Matlab to implement the proposed scheme with adaptive step size integration with $\Delta X = 5$ km or $\Delta X = 2$ km. Solution required between 20 s to 10 min on a standard MacBook Pro 2016 laptop.

Table 1: Model parameters

Param.	**Description**	**Value**
γ	Num. charging slots	2
s	Erlang stages	4
$v_{\max}$	Maximum speed	130 km / h
v_{ave}	Average speed	100 km / h
λ	Electric cars arrival rate	1 car / h
B	Battery capacity (km)	250 km
r_b	Basic energy consumption (km/h)	10 km / h
r_c	Charging rate (km / h)	200 km / h
σ_1, σ_2, σ_3	Parameters of the charging model	$0.68, 0.995, 1.0$
η	Threshold for the battery level	80 km

6 Numerical Results

We fix the number of slots to $\gamma = 2$ for every charging station. To study how the model captures the evolution of the system, we start focusing on policy 4), assigning a threshold $\eta = 80$ km. Figure 4 shows the main state probabilities: charging, waiting, success and failure. On Figure 4 we have also reported the average battery percentage $\bar{\beta}(t)$ at time t, and the average number of segments $\bar{\phi}(t)$ already driven at time t, where $\phi(i)$ is the highway segment corresponding to state $\mathbf{m}_i$. The two quantities $\bar{\beta}(t)$ and $\bar{\phi}(t)$ are expressed in Equation (16) and are conditioned on the fact that the tagged BEV reaches its destination, and on the probability that it is still traveling at time t. Let us call $\pi_{dest}(t)$ the probability that the car has succesfully reached its destination at time t, and $\pi_{fail}(t)$ the probability that the car has run out of battery while traveling on a segment. Then we have:

$$\bar{\beta}(t) = \frac{1}{B}\left[\sum_i \int_{\beta=0}^{B} \beta\, \pi_i(t,\beta)\, d\beta\right] (1 - \pi_{dest}(t) - \pi_{fail}(t))^{-1}$$
$$\bar{\phi}(t) = \frac{1}{K}\left[\sum_i \int_{\beta=0}^{B} \phi(i)\pi_i(t,\beta)\, d\beta\right] (1 - \pi_{dest}(t))^{-1} \tag{16}$$

From the plot, it is possible to visualize when the car stops, and how long it has to wait for charging the battery. It is interesting to note that the probability

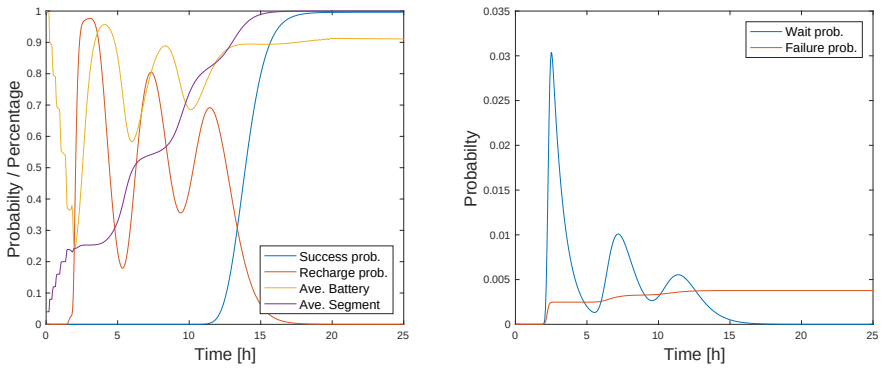

(a) (b)

Fig. 4: States evolution: a) success probability, charging probability, average battery percentage and average number of segments driven at time; b) waiting probability and failure probability

of charging the battery becomes negligible as the probability of reaching the

destination becomes higher. The "staircase" trend of "Ave. Battery" and "Ave. segment" curves, observable at time t $<$ 2h, is due to the embedded process behavior. In particular to the impulsive battery level reduction l_ϕ that occurs at discrete times when the vehicle reaches the next service station, modeled by the firing of transition $SEGMENT(\phi)$ in Fig 2.

We then start comparing the various policies, showing the probability of unsuccessful arrival at destination in Figure 5a), and the trip duration distribution conditioned on a successful arrival in Figure 5b). Policy 2), which stops the car at every charging point, has basically no probability of failing, but it experiences an extremely long trip duration. Conversely, policy 1) that stops the car only when absolutely needed has the worst reliability. Its response time is not one of the best either, since it stops independently on the queue at the station where the battery level becomes too small. Policy 3), as expected, places itself between the two. The more advanced policies 4) and 5) have a much shorter traveling time, but policy 5), which anticipates the recharge, shows a lower failure probability than policy 4).

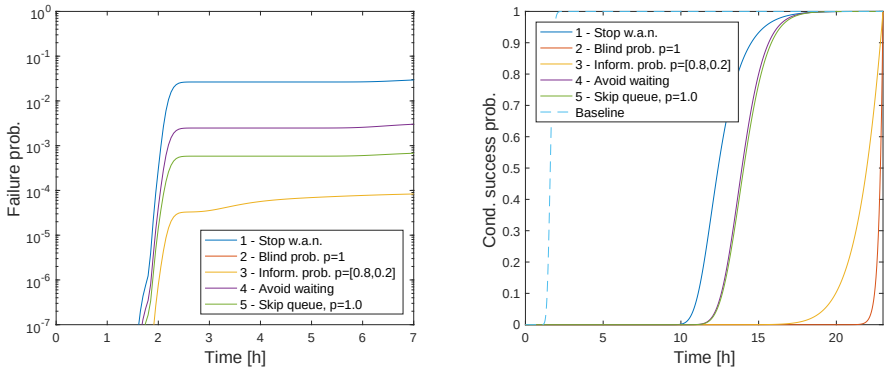

(a) (b)

Fig. 5: a) Failure probability and b) conditioned success probability, as function of time for the 4 considered policies

Figure 6a) shows the average battery level as a function of time. for the different decision policies. Policies 2) and 3) induce frequent stops and recharges and the battery power is not well exploited since the charge is almost always at the maximum level. Policy 1) depletes the battery almost completely before charging. For Policies 4) and 5) (whose curves are almost indistinguishable) the battery depletion and then the stops to charge are well visible; the two policies perform an early charge, more or less in the same station.

Figure 6b) for the only Policy 4) shows the effect on the battery cycles of the speed of the car. The increased average speed has two competing effects.

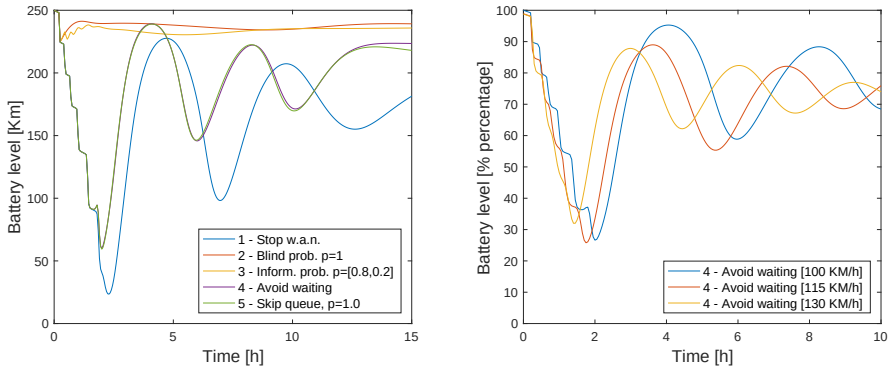

(a) (b)

Fig. 6: a) Average battery level versus time for the considered policies and b) Average battery level versus average speed for Policy 4)

The battery depletion rate increases almost linearly with the speed [22], but since driving a segment takes a shorter time, also the battery consumption due to the services (AC, sound, etc.) is lower. The combined effect in Figure 6b) shows that at increased speed the recharge must be done more frequently. The curves in Figure 6b) have been obtained by setting $v_{\max} = 140\,km/h$ and $v_{ave} = 100, 115, 130\,km/h$.

As explained in Section 4.2, Policies 4) and 5) require a safety threshold η to decide their stopping interval. Figure 7 shows the average trip time and the failure probability for policies 4) and 5) under different thresholds $\eta \in [20 \ldots 120]$ km. While the failure probability increases as the margin decreases, as expected, the average trip time has a non-linear and non-monotonic behavior, even if it tends to increase with η. This tendency is motivated from the fact that by stopping earlier there is a higher chance of requiring an additional stop. Non-monotonic behavior is instead caused by the non uniform position of service stations along the road. In some cases, increasing the margin can have a positive effect: arriving at a station with a larger remaining battery capacity decreases the stopping time. If this does not increase the required number of stops, it has the effect of reducing the traveling time. By combining both measures with appropriate goal-dependent weights, the proposed model can thus be used to find the value of η which gives the best trade-off between traveling speed and failure probability depending on the position of the charging points along the trip.

7 Conclusions

This paper has explored a new line of research by analyzing a system composed by electric vehicles, immersed in a traffic flow, on a real highway, and their

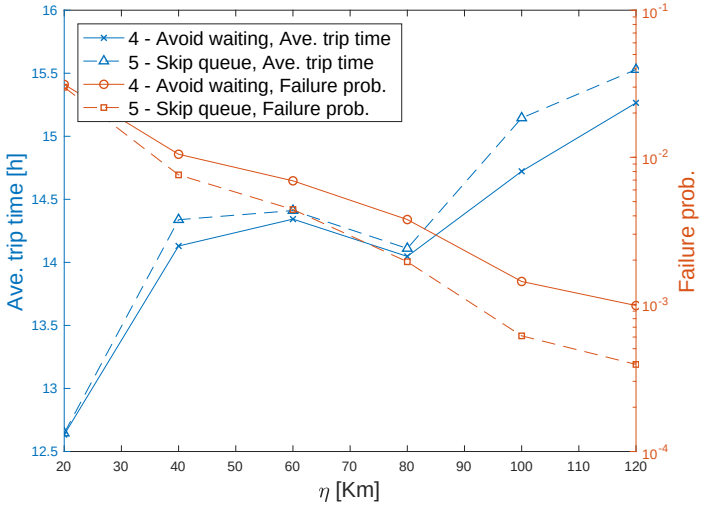

Fig. 7: Average traveling time and failure probability for policies 4) and 5) under different margins $\eta \in [20 \dots 120]$.

interaction with the related charging infrastructure. The balance between the probability of successfully completing the itinerary versus the time required to complete the trip, that is influenced by the number of stops and the state of the queue at the charging stations, has been examined under different charging decision policies. The described system has been modeled and analyzed using stochastic fluid models, and in particular, Fluid Stochastic Petri Nets. Although results are still preliminary, the paper shows the appropriateness of the considered technique for studying the performance and the reliability of the proposed system.

The model is predisposed to be extended in different directions. More realistic traffic condition, in which the speed of the car flow can be modulated according to the traffic intensity, and the battery depletion rate is sensitive to the speed of the tagged BEV. The incorporation of chargers with different characteristics that modify the nonlinear charging profile of the battery. The inclusion of the probability of the charging station to be up or down, and the adaptation of the stopping decision policies. Further the decision policy can benefit by the availability of system level controllers (i.e., an app) that informs the driver of unavailable or free slots along the way.

The model investigated in this paper can be proposed as a building block for an optimization strategy aimed at finding the best policy parameters for a given road. Further, the analysis of charging decision policies can provide suitable algorithms to be implemented on board, mainly in view of the possible new generation of autonomous EVs.

Appendix

In Table 2 the location of the service stations along A14 Bologna to Taranto is shown. In particular: the name of the service stations (column 2), the length of the segments (column 3) together with the progressive distances from the start (column 4) and to the end (column 5).

Table 2: Location of service stations along A14 Bologna to Taranto

	Station	**Distances [km]**		
ϕ	**Name**	**segment**	**from start**	**to end**
0	Bologna	0	0	743.4
1	La Pioppa	2.3	2.3	741.1
2	Sillaro	35.1	37.4	706
3	Santerno	22.1	59.5	683.9
4	Bevano	30	89.5	653.9
5	Rubicone	21.8	111.3	632.1
6	Montefeltro	22.3	133.6	609.8
7	Foglia	25.3	158.9	584.5
8	Metauro	27.3	186.2	557.2
9	Esino	22.5	208.7	534.7
10	Conero	30.3	239	504.4
11	Chienti	24.9	263.9	479.5
12	Piceno	26.9	290.8	452.6
13	Tortoreto	32.9	323.7	419.7
14	Vomano	16.6	340.3	403.1
15	Torre Cerrano	22.8	363.1	380.3
16	Alento	30.8	393.9	349.5
17	Sangro	34.9	428.8	314.6
18	Trigno	29.8	458.6	284.8
19	Torre Fantine	15	493.5	269.8
20	S.Trifone	19.9	517.51	249.9
21	Gargano	48.73	542.23	201.17
22	Le Saline	44.94	587.17	156.23
23	Canne Battaglia	33.19	620.36	123.04
24	Dolmen Di Bisceglie	24.05	644.41	98.99
25	Murge	27.03	671.44	71.96
26	Le Fonti	26.18	697.5	45.78
27	Taranto	36.78	743.4	0

References

1. International Energy Agency. Global energy review 2021. https://www.iea.org/reports/global-energy-review-2021, 2021 (access 2021-Nov).
2. International Energy Agency. Global EV outlook 2020. https://www.iea.org/reports/global-ev-outlook-2020, 2020 (accessed 2021-Nov).

3. J. García-Villalobos, I. Zamora, J.I. San Martín, F.J. Asensio, and V. Aperribay. Plug-in electric vehicles in electric distribution networks: A review of smart charging approaches. *Renewable and Sustainable Energy Reviews*, 38:717–731, 2014.
4. A. Sbihi and R.W. Eglese. Combinatorial optimization and green logistics. *4OR*, 5:99–116, 2014.
5. S. Erdoğan and E. Miller-Hooks. A green vehicle routing problem. *Transportation Research Part E: Logistics and Transportation Review*, 48(1):100–114, 2012.
6. A. Khaksari, G. Tsaousoglou, P. Makris, K. Steriotis, N.s Efthymiopoulos, and E. Varvarigos. Sizing of electric vehicle charging stations with smart charging capabilities and quality of service requirements. *Sustainable Cities and Society*, 70:102872, 2021.
7. A. Dupont, Y. Hayel, T. Jiménez, O. Beaude, and C. Wan. Coupled queueing and charging game model with energy capacity optimization. In *Performance Engineering and Stochastic Modeling (ASMTA 2021)*. Springer - LNCS, 2021.
8. Abdullah Al-Karakchi, Ghanim Putrus, and Ridoy Das. Smart ev charging profiles to extend battery life. In *2017 52nd International Universities Power Engineering Conference (UPEC)*, pages 1–4, 2017.
9. M. Gribaudo, M. Sereno, A. Horváth, and A. Bobbio. Fluid stochastic Petri nets augmented with flush-out arcs: Modelling and analysis. *Discrete Event Dynamic Systems*, 11 (1/2):97–117, January 2001.
10. T. Erdelić and T. Carić. A survey on the electric vehicle routing problem: Variants and solution approaches. *J Advanced Transportation*, Article ID 5075671, 2019.
11. I. Kucukoglu, R. Dewil, and D. Cattrysse. The electric vehicle routing problem and its variations: A literature review. *Computers & Industrial Engineering*, 161:107650, 2021.
12. Simona Mancini. The hybrid vehicle routing problem. *Transportation Research Part C: Emerging Technologies*, 78:1–12, 2017.
13. Michael Schneider, Andreas Stenger, and Dominik Goeke. The electric vehicle-routing problem with time windows and recharging stations. *Transportation Science*, 48(4):500–520, 2014.
14. Maurizio Bruglieri, Ferdinando Pezzella, Ornella Pisacane, and Stefano Suraci. A variable neighborhood search branching for the electric vehicle routing problem with time windows. *Electronic Notes in Discrete Mathematics*, 47:221–228, 2015.
15. Alejandro Montoya, Christelle Guéret, Jorge E Mendoza, and Juan G Villegas. The electric vehicle routing problem with nonlinear charging function. *Transportation Research Part B: Methodological*, 103:87–110, 2017.
16. Maurizio Bruglieri, Simona Mancini, Ferdinando Pezzella, and Ornella Pisacane. A path-based solution approach for the green vehicle routing problem. *Computers & Operations Research*, 103:109–122, 2019.
17. M. Keskin, G. Laporte, and B. Çatay. Electric vehicle routing problem with time-dependent waiting times at recharging stations. *Computers & Operations Research*, 107:77–94, 2019.
18. J.F. Meyer. On evaluating the performability of degradable systems. *IEEE Transactions on Computers*, C-29:720–731, 1980.
19. K.Trivedi and V. Kulkarni. FSPNs: fluid stochastic Petri nets. In *Proc 14-th Int Conference on Application and Theory of Petri Nets*, pages 24–31, Chicago, 1993.
20. Graham Horton, Vidyadhar G. Kulkarni, David M. Nicol, and Kishor S. Trivedi. Fluid stochastic petri nets: Theory, applications, and solution techniques. *Eur. J. Oper. Res.*, 105(1):184–201, 1998.
21. A. Bobbio. System modelling with Petri nets. In Colombo andSaiz de Bustamante, editor, *System Reliability Assessment*, pages 103–143. Kluwer Academic, 1990.

22. Florent Grée, Vitaliia Laznikova, Bill Kim, Guillermo Garcia, Tom Kigezi, and Bo Gao. Cloud-based big data platform for vehicle-to-grid (v2g). *World Electric Vehicle Journal*, 11(2), 2020.
23. K. Trivedi and A. Bobbio. *Reliability and Availability Engineering: Modeling, Analysis, and Applications*. Cambridge University Press, 2017.
24. János Sztrik. Basic queueing theory: Foundations of system performance modeling. *University of Debrecen, Faculty of Informatics*, 193, 2016.